(Received 6 June 2024, Accepted 13 November 2024, Scheduled 29 November 2024)

Complementary Folded Line Metamaterial Loaded MIMO Antenna for S-Band Applications

Yugender Mood* and Ramasamy Pandeeswari

Department of Electronics and Communication Engineering, National Institute of Technology Thuvakudi, Tiruchirappalli 620015, Tamilnadu, India

ABSTRACT: This paper introduces a MIMO antenna featuring a complementary folded-line metamaterial (CFL-MTM) design, It wants to reduce mutual interaction among very close microstrip patch antenna components. The antenna elements have an edge-to-edge spacing of roughly $0.0933\lambda_0$ (7 mm). By integrating CFL-MTM elements into the antenna structure, the antenna achieves negative permittivity and permeability characteristics, resulting in a compact size of $37 \times 44 \times 1.6\,\text{mm}^3$. The antenna is suitable for S band applications, covering a bandwidth of approximately 3.121–4.277 GHz (1156 MHz). The incorporation of CFL-MTM results in a negative refractive index area, which effectively controls and reduces mutual coupling between the antenna parts. The antenna's dimension is optimized by keeping the CFL-MTM smaller than the resonant wavelength. Furthermore, the characteristics of the suggested MIMO antenna, such as ECC, CCL, and TARC, are assessed to show that it is suitable for S-band applications.

1. INTRODUCTION

Multiple Input Multiple Output (MIMO) antennas are becoming more essential in wireless communication systems because they leverage multipath propagation for both transmitting and receiving information, therefore enhancing data transmission efficiency. Unlike regular Single Input Single Output (SISO) antennas, MIMO systems use several antennas on both the transmitter & receiver ends. Specifically, for 5G mobile applications, a wideband decoupled eight-element MIMO antenna is created by positioning four pairs of antennas on each side of the frame. These antennas use spatial diversity to transmit multiple data signals simultaneously, enhancing both system reliability and throughput. This makes MIMO technology essential for modern high-speed wireless communication [1]. In a MIMO system, densely packed antenna arrays reduce the distance between antennas. Mutual coupling occurs when the distance is less than half of the free space wavelength ($\lambda/2$. Mutual coupling is the electromagnetic relationship between antenna arrays which affects the current in each antenna by considering both individual and nearby antennas. This interaction impacts antenna properties such as radiation, reflection, radar cross-section, and signal-to-interference noise ratio, and is determined by antenna efficiency and isolation [2]. The implementation of cut-side patches and EBG (Electromagnetic Band Gap) structures reduces interference and improves the overall performance of the antenna array. It is especially important for complex communication systems that need excellent performance in tightly packed antenna arrays [3]. A metamaterial polarization-rotator wall can efficiently eliminate the mutual coupling between antennas in an array. The idea is critical for millimeter-wave communication systems, where mutual coupling can severely impair signal quality and reliability of the system [4].

The deployment of the modified serpentine structure effectively minimizes interference between antennas in the array, enhancing signal quality and system reliability. It will contribute to the development of advanced antenna designs for wireless communication systems, particularly in applications requiring robust MIMO performance, such as mobile communication and wireless networks [5]. Electromagnetic Band Gap (EBG) structures are used to reduce mutual coupling effects in MIMO systems. By strategically incorporating EBG elements, the authors can achieve improved isolation between antennas, leading to enhanced system performance and reliability. This will be used in optimizing MIMO antenna systems for various wireless communication applications, emphasizing the importance of reducing mutual coupling for efficient signal transmission and reception [6]. The isolation between antennas in compact arrangements is crucial for applications where antennas must be placed closely together. By utilizing meander line resonators, we can effectively mitigate mutual coupling effects, improving the performance and reliability of the antenna system. This will address the challenges related to interference and signal integrity in closely spaced antenna arrays [7]. Using metamaterials and a novel complementary folded-line metamaterial (CFL-MTM) arrangement, we can significantly isolate antenna components, improving the overall performance of the MIMO system [8]. The performance of patch antenna arrays is improved by mitigating interference between adjacent elements. The use of a Unit-Cell Electromagnetic Band Gap (UC-EBG) superstrate effectively enhances isolation, leading to better antenna performance and system reliability and valuable insights into optimizing antenna array designs, particularly

* Corresponding author: Yugender Mood (yuginaik437@gmail.com).

in applications where mutual coupling can impact signal quality and communication efficiency [9]. A MIMO antenna design uses Split Ring Resonator (SRR) metamaterial and Coplanar Waveguide (CPW) feeding. This study contributes to advancements in antenna technology for sub-6 GHz 5G applications, leveraging innovative materials and feeding techniques to enhance performance and efficiency [10]. The use of a dumbbell EBG structure proves to be effective in mitigating the interference between antenna elements, leading to better overall performance and reliability of the antenna system and the development of advanced techniques for optimizing microstrip antenna arrays, particularly in applications requiring high performance and low mutual coupling [11]. By implementing innovative techniques, we can effectively mitigate interference, enhance isolation between antennas, and improve overall system performance. This research advances MIMO antenna designs for WLAN applications, where efficient communication and reduced mutual coupling are crucial for reliable wireless connectivity. This paper presents an Asymmetric Coplanar Waveguide (ACPW)-fed CFL-MTM inspired wideband MIMO antenna designed specifically for S-band applications. The proposed design leverages the unique properties of metamaterials to achieve significant enhancements in antenna performance, including improvements in gain, isolation, and beam steering capabilities. Through detailed numerical simulations and experimental validations, the effectiveness of the design is demonstrated, showcasing its potential for advanced communication systems. The research contributes valuable insights to the field of antenna design, emphasizing the role of metamaterials in developing efficient, high-performance MIMO antennas suitable for modern wireless communication technologies. This study lays a solid foundation for future work in optimizing metamaterial-based antennas for broader applications in telecommunications and beyond.

2. RELATED WORK

The development of Complementary Folded Line Metamaterial (CFLM) loaded Multiple-Input Multiple-Output (MIMO) antennas for sub-6 GHz applications is a significant area of research, particularly in enhancing wireless communication systems such as those used in 5G networks. This literature review explores key studies in this field, highlighting advances in design techniques, performance improvements, and the practical implications of these innovations.

Simovski investigated the electromagnetic properties of grids composed of conducting Ω particles, examining the reflection and transmission characteristics of plane waves interacting with these grids, along with the dispersion properties of Ω electromagnetic crystals. Detailed analysis and theoretical modeling reveal how these structures influence wave propagation, offering insights into the design of advanced materials with tailored electromagnetic responses [12]. This study investigates the electromagnetic properties of grids composed of conducting Ω particles, examining the reflection and transmission characteristics of plane waves interacting with these grids, along with the dispersion properties of Ω electromagnetic crystals. Detailed analysis and theoretical modeling reveal how these structures influence wave propagation, offering insights into the design of advanced materials with tailored electromagnetic responses [2]. In the context of phase shifters, Saadoun and Engheta presented a novel approach utilizing a pseudochiral or omega (Ω) medium, introducing theoretical and practical considerations for achieving reciprocal phase shifting. The authors explored the electromagnetic properties of the Ω medium, demonstrating its potential for manipulating phase and polarization of microwave signals. Their findings suggest promising applications in microwave technology, offering a new avenue for developing compact and efficient phase shifters for various communication systems [13]. The unique electromagnetic characteristics of Left-Handed Metamaterials (LHMs), which exhibit negative refraction and can reverse the direction of energy flow, were explored by Kondori et al. Through numerical simulations, the authors analyzed how these materials can be designed and optimized for practical applications, particularly examining the behavior of Split-Ring Resonator (SRR) arrays. These arrays are crucial in creating LHMs due to their ability to induce negative magnetic permeability, providing significant insights into the development of metamaterials with tailored electromagnetic responses for advancements in telecommunications and imaging systems [14]. Addressing the growing demand for compact and efficient antennas with broad frequency ranges, Daniel integrated Electric-LC (ELC) unit cells into their design to achieve a negative permeability response, enhancing the antenna's bandwidth and overall performance. The research included detailed numerical simulations and experimental validations, demonstrating the effectiveness of this approach. This work contributes to the advancement of antenna technology by combining the benefits of metamaterials with practical application potential, highlighting significant improvements in size reduction and frequency versatility [15]. In the realm of 5G technology, Khan et al. developed an innovative antenna design leveraging a metamaterial-inspired element to achieve enhanced performance characteristics. By incorporating circular polarization and wideband capabilities, the antenna provides robust and efficient signal transmission and reception, crucial for the dense and high-speed communication environments envisioned for 5G networks. Comprehensive numerical simulations and experimental results validated their design, demonstrating its effectiveness in meeting the stringent requirements of modern wireless communication systems. This work represents a significant advancement in MIMO antenna technology, offering a promising solution for next-generation 5G mmWave applications [16]. Yusuf and Gong focused on beamsteering techniques in MIMO antenna arrays, achieving beam steering capabilities without the need for expensive and complex phase shifters typically used in phased arrays. By utilizing mutual coupling and reactive loading, they simplified the design and significantly reduced the overall cost. Detailed experimental results demonstrated the effectiveness of their approach in steering the antenna beam, highlighting its potential for applications in wireless communication systems where cost and simplicity are crucial factors. This study provides valuable insights into the design of efficient and affordable phased array antennas, making advanced beam

steering technology more accessible for various practical uses [17]. Fan explored the theoretical foundations, design methodologies, and practical implementations of non-Foster circuits integrated into metamaterial structures. His rigorous analysis and experimental validation demonstrated how these active metamaterials could enhance the performance of various electromagnetic devices, including antennas and filters, by broadening their operational bandwidth and improving overall efficiency. This work contributes valuable knowledge to the field of metamaterials, highlighting the potential of non-Foster techniques to revolutionize the design and application of high-frequency components in advanced communication systems [18].

Markos and Soukoulis presented a research that focused on the unique electromagnetic characteristics of Left-Handed Metamaterials (LHMs), which exhibited negative refraction and can reverse the direction of energy flow. By employing numerical simulations, the authors analyzed how these materials can be designed and optimized for practical applications. Specifically, they examined the behavior of Split-Ring Resonator (SRR) arrays, which are crucial components in creating LHMs due to their ability to induce negative magnetic permeability. The findings provide significant insights into the development of metamaterials with tailored electromagnetic responses, paving the way for advancements in various technological fields such as telecommunications and imaging systems [19]. Le et al. presented an approach that leverages the unique properties of metamaterials to enhance antenna performance, specifically targeting improvements in gain and beam steering capabilities. The planar folded-line configuration enables the antenna to achieve significant directional control and high efficiency, making it suitable for advanced communication systems. The authors provided detailed simulations and experimental results to validate their design, demonstrating substantial performance gains compared to traditional antenna structures. Their findings underscore the potential of metamaterials in creating more efficient and adaptable antennas, contributing valuable insights to the field of antenna design and metamaterials. This research lays the groundwork for future developments in high-performance antenna systems, particularly for applications requiring precise beam control and high gain [20]. An eight-element tightly stacked antenna was proposed by Uddin et al., with switchable feeding through a microstrip line, steering a three-bit beam from an antenna array at 28 GHz millimeter wave. The study addresses the need for adaptable and efficient antenna systems in the rapidly evolving field of 5G communications. By integrating a 3-bit phase shifter into the antenna array, the authors achieved precise control over the beam direction, enabling dynamic reconfiguration to optimize signal coverage and strength. The corporate-fed design ensures uniform power distribution across the array elements, enhancing overall performance. Detailed simulations and experimental results validated the effectiveness of their design, demonstrating significant improvements in beamsteering capabilities and operational flexibility. This work contributes to the advancement of high-frequency antenna technologies, offering a promising solution for next-generation wireless communication systems that require robust and adaptable beamforming capabilities [21]. Lheurette et al. designed Omega-type balanced composite materials with a negative refractive index, to enhance electromagnetic properties for advanced applications. These metamaterials, featuring omega-shaped metallic inclusions, achieved equilibrium between magnetic and electric responses, critical for negative refractive index behavior. Precise microfabrication techniques were utilized to construct these composites, and their properties were validated through detailed simulations and experimental measurements. The results confirm the expected negative refractive index within the targeted frequency range. This advancement opens new possibilities for applications such as miniaturized antennas, improved signal transmission, and innovative optical devices. The balanced nature of the composites contributes to more stable and efficient performance, marking a significant step forward in the field of metamaterials and their practical implementations in electromagnetic and optical engineering [22]. This study aims to develop a comprehensive model to characterize the electromagnetic properties of metamaterials, focusing on their unique behaviors not found in natural materials. The study offers a detailed analysis and theoretical foundation, enabling the design and implementation of circuit metamaterials for a range of applications in electromagnetics. Cui et al. presented a research that contributes significantly to the understanding and development of these advanced materials, paving the way for innovations in fields such as telecommunications, sensing, and imaging technologies [23]. Chen et al. designed Left-handed materials, characterized by a negative refractive index, exhibited unconventional behavior such as reverse Snell's law and backward wave propagation. The authors demonstrated that s-shaped resonators can effectively create left-handed properties, contributing to the development of novel metamaterials with potential applications in advanced optics, telecommunications, and other fields requiring precise control of electromagnetic waves [24].

In this paper, an ACPW-fed CFL-MTM inspired wideband MIMO antenna for S-band applications is presented. ACPW is preferred over traditional CPW due to its greater design flexibility. The paper also includes a comparison of four design stages. The radiating structure of the antenna combines rectangular patches with Complementary Folded-Line Metamaterial (CFL-MTM) etched onto the rectangular patch. This also delves into various performance metrics crucial for MIMO antennas, such as impedance matching, isolation, correlation coefficient, and radiation patterns. Examining these parameters provides insights into optimizing antenna designs to enhance system performance, addressing challenges in multi-band operations and spatial diversity. This work is significant in advancing the development of efficient MIMO antenna systems for diverse wireless applications. In the first stage, a basic rectangular patch is designed, but it performs poorly in terms of reflection coefficient, gain, and voltage standing wave ratio (VSWR), resonating at 4.3 GHz. In the second stage, the rectangular patch is replaced with a CFL-MTM structure, which shifts the resonant frequency to 4.2 GHz and slightly improves all parameters. The third stage introduces a two-element MIMO system with an edge-to-edge distance of 7 mm. In the final proposed stage, the design incorporates the CFL-MTM structure from the

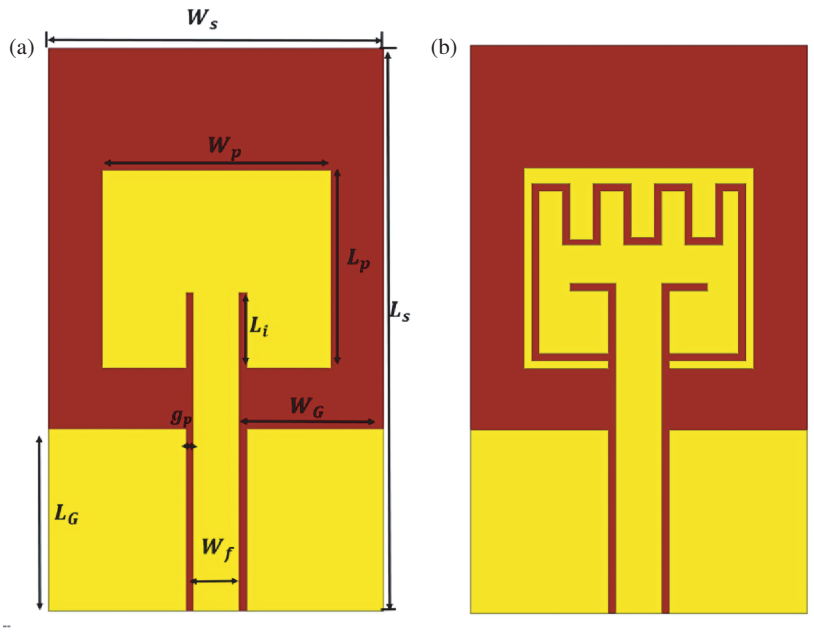

FIGURE 1. Isolated Antenna with and without meta loaded. (a) Isolated Antenna without meta Loaded (Stage-I). (b) Isolated Antenna with meta loaded (Stage-2).

third stage. Each stage is evaluated on performance criteria like gain, bandwidth, VSWR, and S-parameters. The proposed antennas are designed to operate between 3.121 and 4.277 GHz. They have numerous appealing characteristics, including large bandwidth, high gain, and perfect VSWR, making them good choices for S-band applications. Additionally, the proposed antenna outperforms existing designs with a smaller decoupling structure, lower edge-to-edge distance, reduced envelope correlation coefficient (ECC), channel capacity loss (CCL), and total active reflection coefficient (TARC) values, and higher diversity gain (DG). Overall, the proposed antenna is well suited for S-band applications.

The remaining sections of this paper are structured as follows. Section 2 provides a detailed discussion of approaches for improving isolation among MIMO antenna elements and explores various strategies for decreasing mutual coupling. In Section 3, the proposed antenna design is elaborated upon, covering the four different stages of development. Section 4 delves into the design of the CFL-MTM and the extraction of its parameters. Following that, in Section 5, the simulation results are presented and discussed, including a comparison of all the basic parameters of the antenna. Section 6 focuses on discussing MIMO antenna parameters such as ECC, DG, TARC, and CLL. Section 7 includes measurement results and associated discussion. Finally, in Section 8, the paper finishes by summarizing its results and contributions.

3. PROPOSED ANTENNA DESIGN

The schematic view of an isolated antenna along with its dimensions is shown in Fig. 1(a) and 1(b). The antenna design is intended for a low-cost FR-4 substrate with a height of 1.6 mm, a dielectric constant (ϵ_r) of 4.4, and a loss tangent $(\tan\delta)$ of 0.025. The physical dimensions of the stage-I isolated antenna are $(W_s = 22)$ mm and $(L_s = 37)$ mm at 4 GHz. For extremely small antennas, high reactance and low radiation efficiency create major impedance matching issues. To overcome this, an Asymmetric Coplanar Waveguide (ACPW) feeding system is used, which improves design flexibility and smooth impedance matching. To achieve 50-ohm impedance matching, a feed line of width $(W_f = 3)$ mm and length $(L_i = 5)$ mm is placed on top of the substrate. The symmetric ground planes have diameters of 9 mm (W_G), 12 mm (L_G), and 3 mm (S). The symmetric ground plane and center signal strip are separated by $(g_p = 0.5)$ mm.

In the following stage, the suggested CFL-MTM MIMO antenna is printed on an FR-4 substrate with a relative permittivity of 4.4 and thickness of 1.6 mm. The MIMO antenna substrate has a total width of 37 mm (W_M) and a length of 44 mm (L_M). In the simulation, we use a CPW feeding width of 6 mm. The suggested antenna is energized via a 50-ohm transmission line with a width of 3 mm (W_f). Figs. 2(a) and 2(b) depict the fourth stage of the MIMO antenna.

An investigation into the properties of the complementary folded-line (CFL) structure, compared to conventional antennas, has been conducted by incorporating CFL into the antennas. Inspired by this, CFL-based microstrip MIMO antennas have been designed to operate in the 3.121–4.277 GHz range, suitable for broadband wireless applications such as S-band applications.

The research methodology comprises several steps to ensure meaningful results. Firstly, the CFL design includes complementary split-ring resonators (CSRRs) and LC lumped elements. Following that, a single rectangular microstrip patch antenna is created. The CFL structure is then combined into a single microstrip patch antenna. The CFL metamaterial construction and microstrip patch antenna are described as follows.

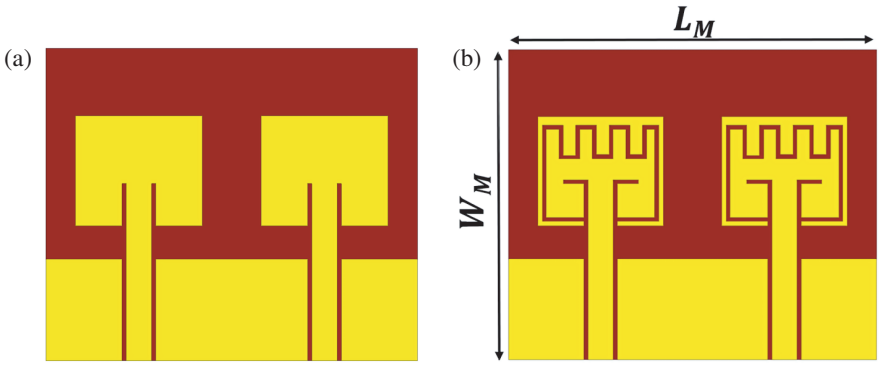

FIGURE 2. MIMO Antenna with/without meta loaded. (a) Stage-3 as MIMO Antenna without meta Loaded. (b) Stage-4 as MIMO Antenna with meta loaded.

Finally, the transition to a MIMO antenna with and without the CFL-MTM loaded patch is addressed using simulation and measurement information.

The simulations were carried out using Ansys HFSS software. All designs used an FR-4 substrate with 1.6 mm thickness, 4.4 dielectric constant, and 0.025 loss factor.

4. COMPLEMENTARY FOLDED-LINE METAMATERIAL DESIGN

The proposed Complementary Folded-Line Metamaterial (CFL-MTM) unit cell was initially simulated to investigate its metamaterial properties. The structure of the proposed CFL-MTM unit cell is depicted in Fig. 3. This CFL-MTM unit cell will be utilized to load the antenna's top plane and is predicted to have left-handed metamaterial (LH-MTM) features. The key dimensions of the CFL-MTM unit cell are summarized in Table 1

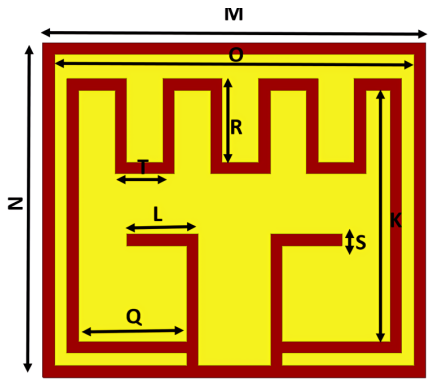

FIGURE 3. Dimension of CFL-LHM unit cell.

To accomplish this, a metallic-cross unit cell designed on an FR-4 substrate was created and simulated as a metamaterial with the Ansys HFSS tool. Perfect boundary conditions were imposed on a unit cell made up of a single metallic cross. A pair of sides of the unit cell (along the y-axis) were assigned perfect electric conductor (PEC) boundary conditions, while the other two sides (along the z-axis) were assigned perfect magnetic conductor (PMC) boundary conditions, as seen in Fig. 4.

TABLE 1. Design Parameters of CFL-MTM.

Symbol	Value (mm)
Length of substate (M)	16
Width of substate (N)	14
Patch length (O)	15
K	10.5
Q	4.5
L	3
T	1.5
R	3.5
split gap S	0.5

The remaining two sides of the unit cell (along the x-axis) were used as wave ports for excitation and radiation purposes. Additional details on the boundary conditions and excitation assignments for the unit cell are provided in Fig. 4.

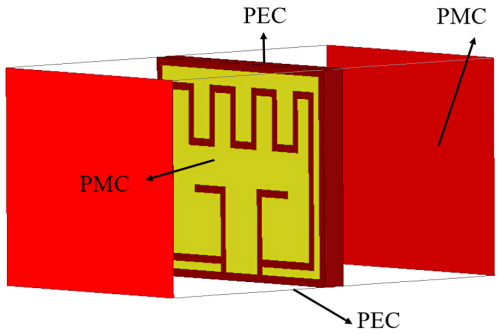

FIGURE 4. CFL-MTM simulation setup.

Figure 6 shows the S-parameter response of a unit cell. Fig. 6 illustrates that the S_{11} and S_{21} parameters overlap at 3.3 GHz and 3.4 GHz, respectively, which indicates that the unit cell structure has a bandgap between 3.3 and 3.4 GHz, where electromagnetic waves are reflected, resulting in negative material characteristics [25, 26].

Moreover, the effective permeability (μ_{eff}) and permittivity (ϵ_{eff}) of the equivalent MTM unit cell are determined using the Nicolson-Ross-Weir (NRW) approach [27]. Equations (1)–

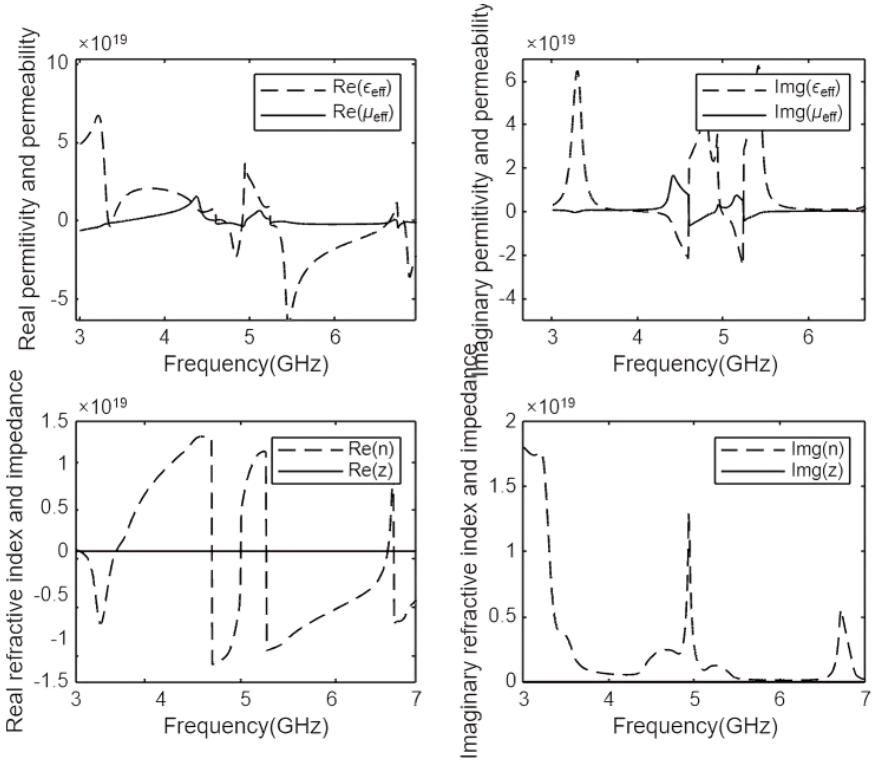

FIGURE 5. Parameter extraction of the FL-LHM unit cell.

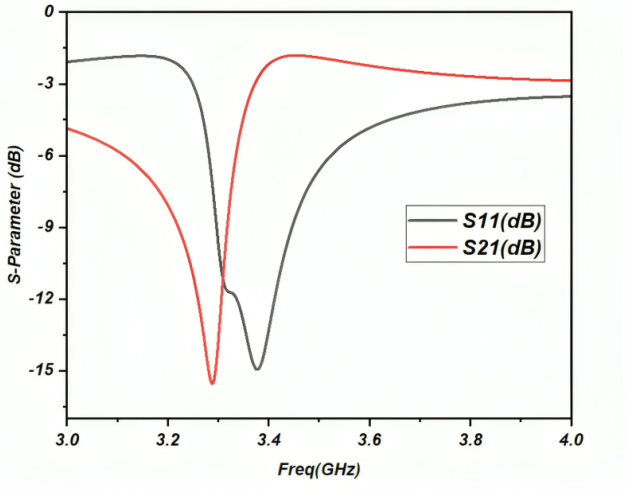

FIGURE 6. Parameter Extraction of the FL-LHM unit cell.

(4) [28] are used to calculate the effective electromagnetic parameters (μ_{eff}) and (ϵ_{eff}) based on the scattering parameters (S_{11}) and (S_{21}). The values of (V_1) and (V_2) represent the sum and difference of the S-parameters, respectively, and are computed using Equations (1) and (2).

$$V_1 = S_{21} + S_{11} \quad (1)$$

$$V_2 = S_{21} - S_{11} \quad (2)$$

$$\mu_{eff} = \frac{2}{jK_{0h}} \cdot \frac{1 - V_2}{1 + V_2} \quad (3)$$

$$\epsilon_{eff} = \frac{2}{jK_{0h}} \cdot \frac{1 - V_1}{1 + V_1} \quad (4)$$

The wave number in free space, k_0, is defined as ω/c, where ω represents the radian frequency and $c = 2\pi f$. The speed of light (c) is 3×10^8 m/s. The corresponding MTM's effective permeability is (μ_{eff}), whereas its effective permittivity is ϵ_{eff}.

The graph in Fig. 5 illustrates the relationship between permittivity and frequency for the CFL-MTM resonator. Based on the results obtained, it is evident that the CFL-MTM resonator exhibits positive permittivity alongside negative permeability and refractive index within the 3–4 GHz range. Furthermore, variations in the split gap of the CFL-MTM resonator may influence the propagation of negativity within the artificial medium by altering its dimensions.

5. SIMULATION RESULTS AND DISCUSSION

The antennas proposed in the preceding section were initially designed using Ansys HFSS and subsequently fabricated using advanced etching techniques on a high-performance substrate. The scattering parameters of the proposed antenna were subsequently measured using a Vector Network Analyzer (VNA), and VSWR results for the four stages were obtained for performance analysis. Following this, a comparison plot of gain versus frequency at different stages was generated, as depicted in Fig. 8. The results from the simulations of the antennas are summarized in this section.

The designed CFL-MTM loaded MIMO antenna is depicted in Fig. 3, displaying the top layer of the board with the patch. Fig. 7 shows the simulated reflection coefficients for four stages. These coefficients are important when the performance of MIMO antennas is analyzed because they indicate how much power is reflected back from the antenna because of the

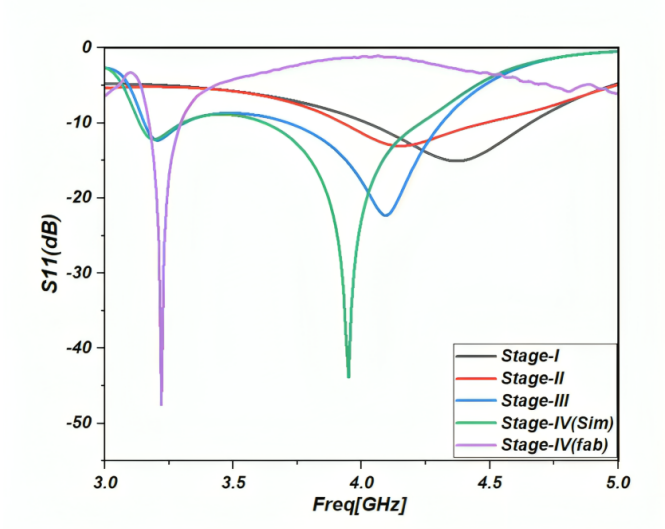

FIGURE 7. Simulated and measured results of the Input reflection coefficient (S_{11}) at different stages (stage-1 to stage 4) of the intended CFL-LHM antenna.

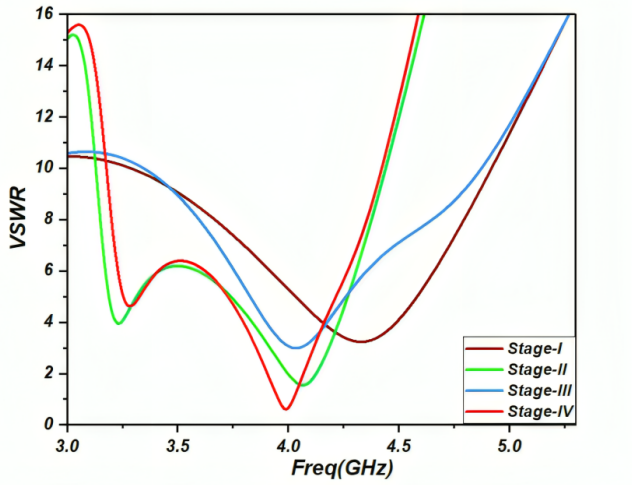

FIGURE 8. Simulated results of the VSWR at different stages (stage-1 to stage-4)of the intended CFL-LHM antenna.

impedance mismatches. Lower reflection coefficients indicate better impedance matching and increased efficiency. Particularly, the suggested antenna resonates in the 3–4 GHz region, with a −10 dB bandwidth around 1.106 GHz. Importantly, the measured results for the fabricated antenna closely match the simulated ones, providing additional validation for the design and simulation accuracy.

The VSWR results at each stage of development for our proposed MIMO antenna system consistently showed values below 1 at 3.121–4.277 GHz, as seen in Fig. 8. This indicates excellent impedance matching and minimal power reflection, validating the effectiveness of our design and tuning processes. The integration and final performance assessments further demonstrated the antenna's robustness and suitability for high-performance MIMO applications.

Figure 9 depicts the simulated gain of antennas at different phases. The antenna gain was evaluated at several phases, with simulated gain values ranging from 0 to 1.98 dB throughout the entire frequency range of 3.121 to 4.277 GHz. At frequencies of 3 GHz and 4.2 GHz, the least measured gain was 1 dB, while the greatest measured gain was 2.28 dB. The radiation efficiency, simulated and displayed in Fig. 9, exceeds 75% over the entire frequency spectrum. The CFL-MTM MIMO antenna's strong performance is further confirmed by its 3D-polar plot for gain (Fig. 10).

The proposed MIMO CFL-MTM loaded patch antenna operates in the S band. Ansys HFSS was utilized for design and optimization, resulting in excellent impedance matching with simulated reflection coefficients consistently below 1. Fabrication measurements validated the simulation's accuracy. The antenna resonated precisely at 4 GHz, boasting a −10 dB bandwidth of approximately 1106 MHz, and maintained low VSWR values, underscoring its efficiency for high-performance MIMO applications in the S band. Table 2 presents the simulation and measurement results for the CFL-MTM MIMO antenna operating at a frequency of 4 GHz.

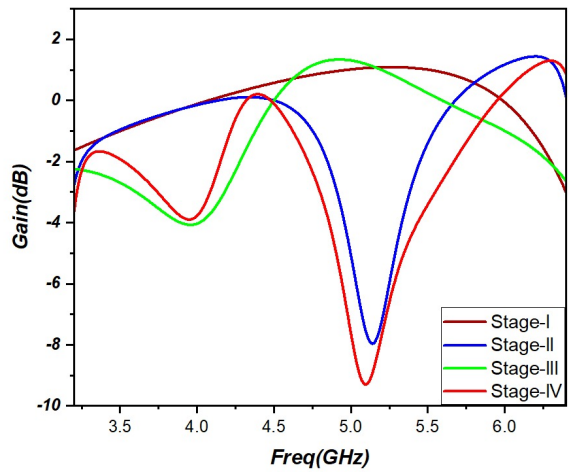

FIGURE 9. Simulated gain vs frequency at different stages (stage-1 to stage-4) of the intended CFL-LHM antenna.

6. MIMO ANTENNA PARAMETERS

Advanced MIMO antenna parameters such as ECC, TARC, DG, and CCL play crucial roles in determining the overall performance of MIMO systems. These parameters influence key aspects such as signal quality, reliability, efficiency, and capacity. Ensuring optimal values for these parameters allows MIMO systems to achieve their full potential, providing enhanced data rates, robust communication links, and efficient spectrum utilization. In the following subsections, we will discuss these MIMO antenna parameters in detail.

6.1. The Envelope Correlation Coefficient (ECC)

The use of numerous antennas or MIMO setups enables further parametric analysis to improve performance. The correlation coefficient (ACC or ECC) addresses the independence of nearby antennas. If the antennas have been determined uncor-

TABLE 2. Results obtained from simulations and measurements of the CFL-MTM MIMO antenna operating at a frequency of $f = 4$ GHz.

Different Stages	Operating frequency (GHz)	$\mathbf{S}_{11}$ (dB)	BW (MHz)	gain (dB)	VSWR
Stage-I	4.3	−18	547	0.67	3.5
Stage-II	4.2	−13	395	-0.39	1.7
Stage-III	4.12	−22	596	2.16	3.3
Stage-VI	4	−43	1106	2.28	0.5
Stage-VI (meas)	3.25	−48	257	3.28	0.88

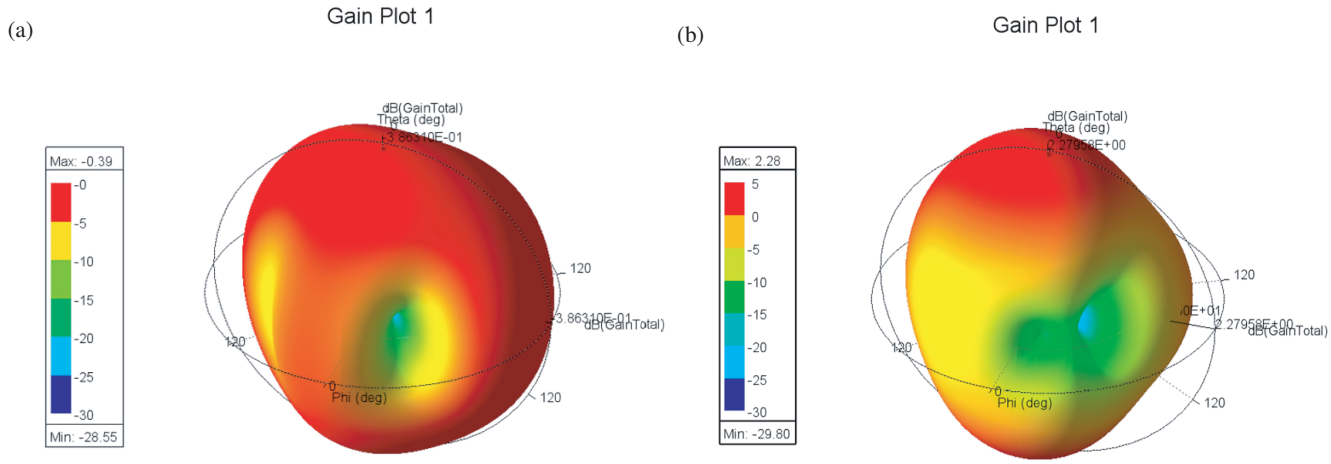

FIGURE 10. Gain plot for MIMO antenna with/without loaded CFL-MTM. (a) 3D polar plot of MIMO Antenna without CFL-LHM Loaded. (b) 3D polar plot of MIMO Antenna with CFL-MTM Loaded.

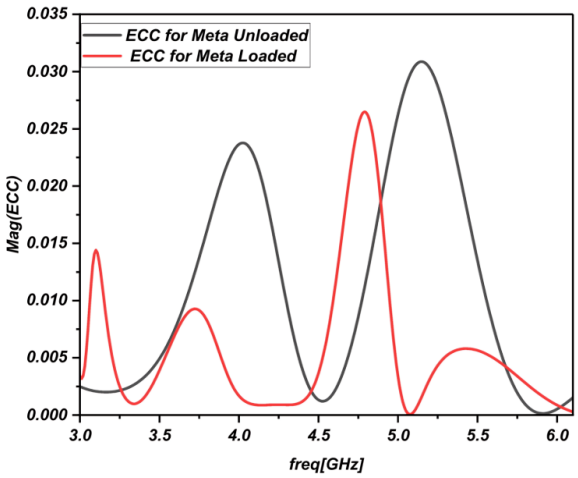

FIGURE 11. The plot between ECC (mag) vs Frequency (GHz).

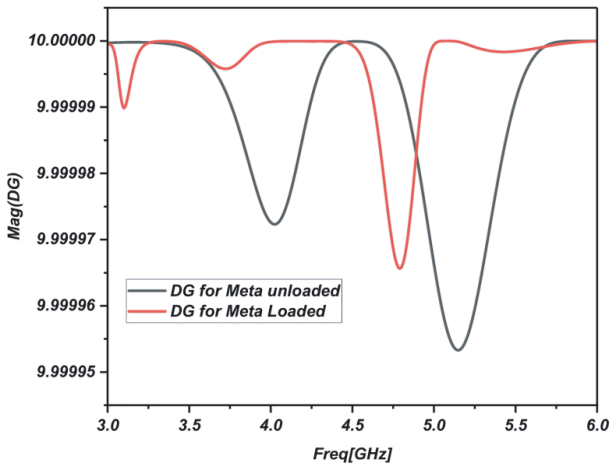

FIGURE 12. The plot between DG (mag) vs Frequency (GHz).

related, they are unsuitable for real-time transmission. When many antennas function at the same time, their radiation patterns interact. This interaction is quantified using the envelope correlation coefficient (ECC) with the formula presented in (5).

$$\mathbf{ECC} = \frac{(|S_{11} * S_{12} + S_{21} * S_{22}|)^2}{(1 - |S_{11}^2| - |S_{21}^2|)(1 - |S_{22}^2| - |S_{12}^2|)} \quad (5)$$

Under ideal conditions, the highest acceptable threshold of ECC (e) is < 0.5 for communicating devices [1]. The suggested MIMO structure has an ECC value of less than 0.020 in the S-band region, as seen in Fig. 11, which plots ECC vs frequency.

6.2. Diversity Gain (DG)

The growth of smart antennas has highlighted the requirement for diversity gain, which is a reduction in fading margin when these reconfigurable antennas are utilized. The formula (6) ex-

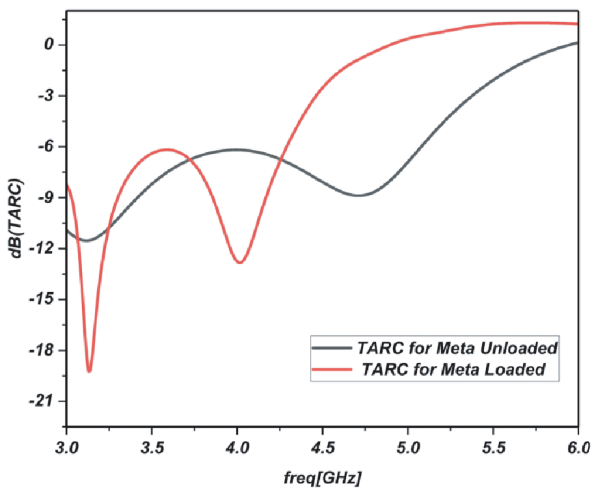

FIGURE 13. The plot between TARC (dB) and frequency (GHz).

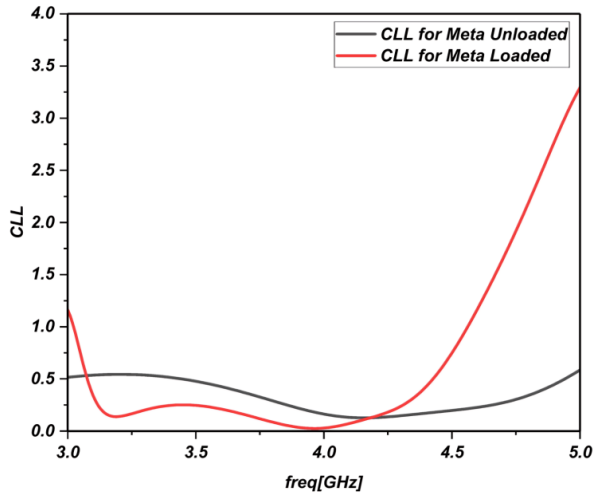

FIGURE 14. The plot between CCL (bps/Hz) and frequency (GHz).

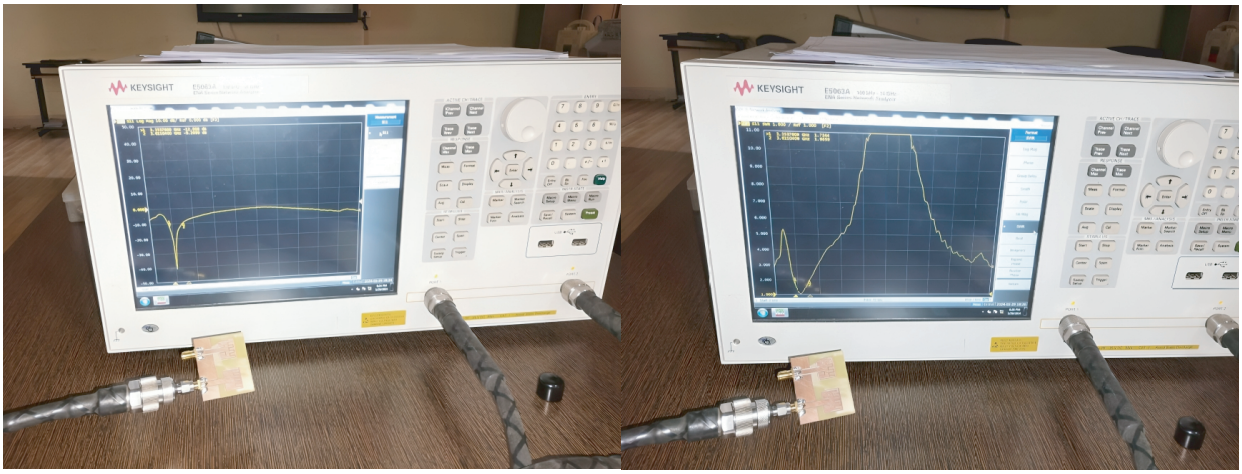

FIGURE 15. Measurements of fabricated antenna.

presses the diversity gain in the MIMO [29] setup.

$$DG = 10\sqrt{1-(ECC)^2} \tag{6}$$

Figure 12 illustrates the diversity plot of the MIMO antenna. The allowed range for variety increase is around 10 decibels. Due to increased ECC performance, the S-band range has a diversity gain of almost 0.1 across the impedance bandwidth. As a result, the developed antenna has a higher correlation with nearby antennas and performs well in diversity.

6.3. Total Active Reflection Coefficient (TARC)

If the design has a single antenna, the return loss parameter is used to evaluate it. TARC is used as an evaluation metric in MIMO configurations, analyzing the return loss of the entire proposed MIMO design while allowing for the antenna's mutual interaction. Equation (7) provides the TARC value.

$$\text{TARC} = \frac{\sqrt{(S_{11}+S_{22})^2+(S_{12}+S_{22})^2}}{\sqrt{2}} \tag{7}$$

The ideal TARC is often less than 0 dB [1]. The TARC value (dB) for the proposed antenna design, shown in Fig. 13, keeps below -3 dB over the entire S-band range.

6.4. Channel Capacity Loss (CCL)

In MIMO antenna's multipath environment, channel capacity affects transmitter and receiver designs. This element should also be addressed while signal degradation is analyzed. Equation (8) describes how the loss of channel capacity is controlled by the S-parameter measurements.

$$CCL = -\log_2(1-S_{11}^2-S_{12}^2) \tag{8}$$

Figure 14 shows a graphical representation of CCL throughout the frequency range. CCL has a peak value of < 0.5, making it acceptable for portable devices with MIMO setup. The CCL value in the intended Narrow Band (NB)-SRR MIMO configuration is less than 0.10 bits/sec/Hz across the 3–4 GHz frequency ranges. As a result, the projected MIMO parameter values are most likely appropriate for S-band applications.

TABLE 3. Comparative analysis of the proposed antenna with other similar works.

Ref.	Technique	Centre Frequency (GHz)	Edge to Edge Distance	Isolation Improvement	FTBR (dB)	ECC	CLL (bps/Hz)
[4]	metamaterial polarization-rotator	60	NA	16	NA	$< 0.1 \times 10^{-}6$	NA
[5]	Serpentine structure	2.45	$0.05\lambda_o$	10–34	NA	< 0.007	NA
[6]	EBG	6	$0.5\lambda_o$	8	NA	< 0.01	NA
[7]	I-shaped resonator	2.8	$0.056\lambda_o$	8–10	NA	NA	NA
[8]	Metamaterial	5.8	$0.135\lambda_o$	9	NA	< 0.1	< 0.05
[9]	UC-EBG	5.56	$0.5\lambda_o$	10	NA	NA	NA
[11]	EBG	7.5	NA	4	NA	NA	NA
[30]	Slotted ground	5.8	$0.33\lambda_o$	40	NA	NA	NA
[31]	U-Shaped resonator	5.4	$0.1\lambda_o$	14	22.1	< 0.1	0.07
This Work	CFL-LHM resonator	4	$0.009\lambda_o$	14	22.1	< 0.1	< 0.01

7. MEASUREMENT RESULT AND DISCUSSION

The fabricated antennas are analyzed with VNA, as shown in Fig. 15. The simulation observations for the CFL-MTM MIMO antenna, especially the S_{11} parameter, are compared to those obtained from built antennas using Keysight Technologies' E5063A Vector Network Analyzer. Fig. 15 depicts a top view of the fabricated antenna structures. The return loss S_{11} (dB) for the first passband is -45 dB around the center frequency of 3.2 GHz, and -22 dB at 6 GHz for the second passband. These antenna characteristics are also appropriate for MIMO configuration operating in the sub-6 GHz frequency region, producing excellent parametric outcomes such as ECC, DG, TARC, and CCL. The comparative analysis of the proposed antenna against similar existing designs is provided in Table 3.

8. CONCLUSION

In conclusion, this paper presents an ACPW-fed CFL-MTM inspired wideband MIMO antenna designed for S-band applications, showcasing significant advancements in MIMO antenna systems. The adoption of ACPW over traditional CPW is highlighted for its greater design flexibility. Through a comparison of four design stages, the study demonstrates the effectiveness of combining rectangular patches with Complementary Folded-line Metamaterial (CFL-MTM) etched onto the rectangular patch. The analysis covers crucial performance metrics for MIMO antennas, including impedance matching, isolation, correlation coefficient, and radiation patterns. These insights are valuable for optimizing antenna designs to enhance system performance, addressing the challenges associated with multi-band operations and spatial diversity. This work represents a meaningful contribution to the development of efficient MIMO antenna systems for diverse wireless applications.

REFERENCES

[1] Sharawi, M. S., "Printed multi-band MIMO antenna systems and their performance metrics," *IEEE Antennas and Propagation Magazine*, Vol. 55, No. 5, 218–232, 2013.

[2] Shams, K. M. Z. and M. Ali, "A CPW-fed inductively coupled modified bow-tie slot antenna," in *2005 IEEE Antennas and Propagation Society International Symposium*, Vol. 3, 365–368, Washington, DC, USA, Jul. 2005.

[3] Mohamadzade, B., A. Lalbakhsh, R. B. V. B. Simorangkir, A. Rezaee, and R. M. Hashmi, "Mutual coupling reduction in microstrip array antenna by employing cut side patches and EBG structures," *Progress In Electromagnetics Research M*, Vol. 89, 179–187, 2020.

[4] Farahani, M., J. Pourahmadazar, M. Akbari, M. Nedil, A. R. Sebak, and T. A. Denidni, "Mutual coupling reduction in millimeter-wave MIMO antenna array using a metamaterial polarization-rotator wall," *IEEE Antennas and Wireless Propagation Letters*, Vol. 16, 2324–2327, 2017.

[5] Arun, H., A. K. Sarma, M. Kanagasabai, S. Velan, C. Raviteja, and M. G. N. Alsath, "Deployment of modified serpentine structure for mutual coupling reduction in MIMO antennas," *IEEE Antennas and Wireless Propagation Letters*, Vol. 13, 277–280, 2014.

[6] Margaret, D. H., M. R. Subasree, S. Susithra, S. S. Keerthika, and B. Manimegalai, "Mutual coupling reduction in MIMO antenna system using EBG structures," in *2012 International Conference on Signal Processing and Communications (SPCOM)*, 1–5, Bangalore, India, Jul. 2012.

[7] Ghosh, J., S. Ghosal, D. Mitra, and S. R. B. Chaudhuri, "Mutual coupling reduction between closely placed microstrip patch antenna using meander line resonator," *Progress In Electromagnetics Research Letters*, Vol. 59, 115–122, 2016.

[8] Iqbal, A., O. A. Saraereh, A. Bouazizi, and A. Basir, "Metamaterial-based highly isolated MIMO antenna for portable wireless applications," *Electronics*, Vol. 7, No. 10, 267, 2018.

[9] Farahani, H. S., M. Veysi, M. Kamyab, and A. Tadjalli, "Mutual coupling reduction in patch antenna arrays using a UC-EBG superstrate," *IEEE Antennas and Wireless Propagation Letters*, Vol. 9, 57–59, 2010.

[10] Mood, Y. and R. Pandeeswari, "A novel SRR metamaterial inspired CPW-fed dual band MIMO antenna for Sub-6 GHz 5G application," *Wireless Personal Communications*, Vol. 130, No. 2, 1277–1293, 2023.

[11] Yu, A. and X. Zhang, "A novel method to improve the performance of microstrip antenna arrays using a dumbbell EBG structure," *IEEE Antennas and Wireless Propagation Letters*, Vol. 2, 170–172, 2003.

[12] Simovski, C. R., "Plane-wave reflection and transmission by grids of conducting Ω-particles and dispersion of Ω electromagnetic crystals," *AEU — International Journal of Electronics and Communications*, Vol. 57, No. 5, 358–364, 2003.

[13] Saadoun, M. M. I. and N. Engheta, "A reciprocal phase shifter using novel pseudochiral or Ω medium," *Microwave and Optical Technology Letters*, Vol. 5, No. 4, 184–188, 1992.

[14] Kondori, H., M. A. Mansouri-Birjandi, and S. Tavakoli, "Reducing mutual coupling in microstrip array antenna using metamaterial spiral resonator," *International Journal of Computer Science Issues (IJCSI)*, Vol. 9, No. 3, 51, 2012.

[15] Daniel, R. S., "Broadband μ-negative antenna using ELC unit cell," *AEU — International Journal of Electronics and Communications*, Vol. 118, 153147, 2020.

[16] Khan, A., Y. He, and Z. N. Chen, "An eight-port circularly polarized wideband MIMO antenna based on a metamaterial-inspired element for 5G mmWave applications," *IEEE Antennas and Wireless Propagation Letters*, Vol. 22, No. 7, 1572–1576, 2023.

[17] Yusuf, Y. and X. Gong, "A low-cost patch antenna phased array with analog beam steering using mutual coupling and reactive loading," *IEEE Antennas and Wireless Propagation Letters*, Vol. 7, 81–84, 2008.

[18] Fan, Y., "Research and design of non-foster active metamaterials," Ph.D. dissertation, Queen Mary University of London, London, UK, 2013.

[19] Markoš, P. and C. M. Soukoulis, "Numerical studies of left-handed materials and arrays of split ring resonators," *Physical Review E*, Vol. 65, No. 3, 036622, 2002.

[20] Le, M. T., Q. C. Nguyen, and T. P. Vuong, "Design of high-gain and beam steering antennas using a new planar folded-line metamaterial structure," *International Journal of Antennas and Propagation*, Vol. 2014, No. 1, 302580, 2014.

[21] Uddin, M. N., M. N. A. Tarek, M. K. Islam, and E. A. Alwan, "A reconfigurable beamsteering antenna array at 28 GHz using a corporate-fed 3-bit phase shifter," *IEEE Open Journal of Antennas and Propagation*, Vol. 4, 126–140, 2023.

[22] Lheurette, E., G. Houzet, J. Carbonell, F. Zhang, O. Vanbesien, and D. Lippens, "Omega-type balanced composite negative refractive index materials," *IEEE Transactions on Antennas and Propagation*, Vol. 56, No. 11, 3462–3469, 2008.

[23] Cui, T.-J., H.-F. Ma, R. Liu, B. Zhao, Q. Cheng, and J. Chin, "A symmetrical circuit model describing all kinds of circuit metamaterials," *Progress In Electromagnetics Research B*, Vol. 5, 63–76, 2008.

[24] Chen, H., L. Ran, J. Huangfu, X. Zhang, K. Chen, T. M. Grzegorczyk, and J. A. Kong, "Left-handed materials composed of only S-shaped resonators," *Physical Review E — Statistical, Nonlinear, and Soft Matter Physics*, Vol. 70, No. 5, 057605, 2004.

[25] Saravanan, M., V. B. Geo, and S. M. Umarani, "Gain enhancement of patch antenna integrated with metamaterial inspired superstrate," *Journal of Electrical Systems and Information Technology*, Vol. 5, No. 3, 263–270, 2018.

[26] Al-Bawri, S. S., M. S. Islam, H. Y. Wong, M. F. Jamlos, A. Narbudowicz, M. Jusoh, T. Sabapathy, and M. T. Islam, "Metamaterial cell-based superstrate towards bandwidth and gain enhancement of quad-band CPW-fed antenna for wireless applications," *Sensors*, Vol. 20, No. 2, 457, 2020.

[27] Costa, F., M. Borgese, M. Degiorgi, and A. Monorchio, "Electromagnetic characterisation of materials by using transmission/reflection (T/R) devices," *Electronics*, Vol. 6, No. 4, 95, 2017.

[28] Nicolson, A. M. and G. F. Ross, "Measurement of the intrinsic properties of materials by time-domain techniques," *IEEE Transactions on Instrumentation and Measurement*, Vol. 19, No. 4, 377–382, 1970.

[29] Jeyakumar, P., A. Ramesh, S. Srinitha, V. Vishnu, and P. Muthuchidambaranathan, "Wideband hybrid precoding techniques for THz massive MIMO in 6G indoor network deployment," *Telecommunication Systems*, Vol. 79, No. 1, 71–82, 2022.

[30] OuYang, J., F. Yang, and Z. M. Wang, "Reducing mutual coupling of closely spaced microstrip MIMO antennas for WLAN application," *IEEE Antennas and Wireless Propagation Letters*, Vol. 10, 310–313, 2011.

[31] Iqbal, A., A. Altaf, M. Abdullah, M. Alibakhshikenari, E. Limiti, and S. Kim, "Modified U-shaped resonator as decoupling structure in MIMO antenna," *Electronics*, Vol. 9, No. 8, 1321, 2020.